LBL-11520
Preprint

Lawrence Berkeley Laboratory
UNIVERSITY OF CALIFORNIA

Physics, Computer Science & Mathematics Division

To be submitted for publication

NUMERICAL MODELING OF TURBULENT FLOW IN A COMBUSTION TUNNEL

A.F. Ghoniem, A.J. Chorin, and A.K. Oppenheim

September 1980

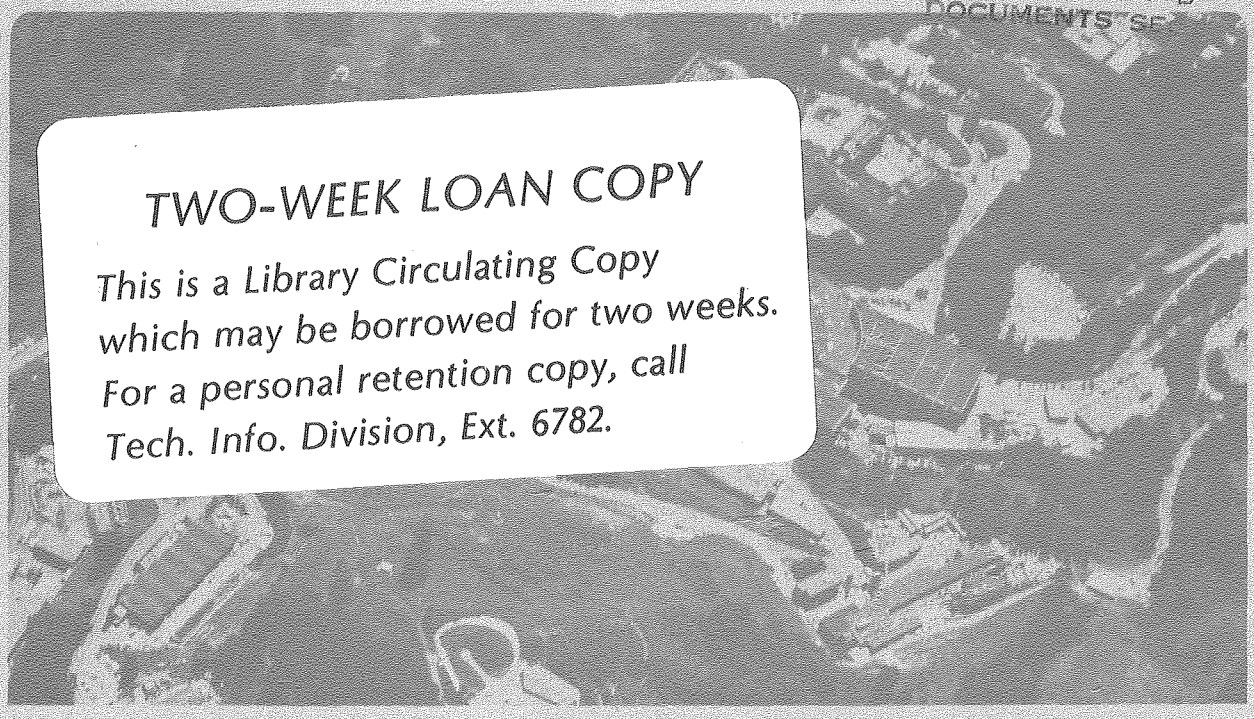

Prepared for the U.S. Department of Energy under Contract W-7405-ENG-48

DISCLAIMER

LBL-11520

NUMERICAL MODELING OF TURBULENT FLOW IN A COMBUSTION TUNNEL

A. F. Ghoniem, A. J. Chorin, and A. K. Oppenheim

Lawrence Berkeley Laboratory
University of California
Berkeley, California 94720

September 1980

NUMERICAL MODELING OF TURBULENT FLOW IN A COMBUSTION TUNNEL*

A. F. Ghoniem, A. J. Chorin, and A. K. Oppenheim

Lawrence Berkeley Laboratory, University of California

Berkeley, CA 94720

ABSTRACT

A numerical technique for the analysis of turbulent flow associated with combustion is presented. The technique utilizes Chorin's RVM (Random Vortex Method), an algorithm capable of tracing the action of elementary turbulent eddies and their cumulative effects without imposing any restriction upon their motion. In the past RVM has been used with success to treat non-reacting turbulent flows, revealing, in particular, the mechanics of large scale flow patterns, the so-called coherent structures. Introduced here is a flame propagation algorithm, also developed by Chorin, in conjunction with volume sources modeling the mechanical effects of the exothermic process of combustion. As an illustration of its use, the technique is applied to flow in a combustion tunnel where the flame is stabilized by a back-facing step. Solutions for both non-reacting and reacting flow fields are obtained, under the restriction of a set of most stringent idealizations, mimicking nonetheless quite

satisfactorily the essential features of turbulent combustion in a lean propane-air mixture that were observed in the laboratory by means of high speed schlieren cinematography.

*This work was supported by the Engineering, Mathematical, and Geosciences Division of the U.S. Department of Energy under contract W-7405-ENG-48, and by the National Aeronautics and Space Administration under NASA Grant NSG-3227.

NUMERICAL MODELING OF TURBULENT FLOW IN A COMBUSTION TUNNEL

CONTENTS

NOMENCLATURE

A – area

c = $(T-T_u)/(T_b-T_u)$, reaction progress parameter or reactedness

d_j – influence factor of a vortex sheet

f = V_b/V_c, fractional volume of burned medium in a cell

F = $d\zeta/dZ$, differential transformation function

h – length of a vortex sheet

h_c – side length of a cell

G – the Green's function

H – width of the channel

k – time step

$\underset{\sim}{L}$ – reference length

i – $\sqrt{-1}$

J_b – number of vortex blobs

J_s – number of source blobs

$\underset{\sim}{n}$ – unit vector normal to solid boundaries

p = $\underset{\sim}{p}/\rho\underset{\sim}{u}_\infty$, non-dimensional pressure

$\underset{\sim}{p}$ – pressure

$\underset{\sim}{r}$ – (x,y), position vector

r_o – blob core radius

R = $\rho\underset{\sim}{u}_\infty H/2\mu$, Reynolds number

$\underset{\sim}{s}$ – unit vector tangential to solid walls

S – normal burning velocity

$\underset{\sim}{t}$ – time

t = $\underset{\sim}{t}\underset{\sim}{u}_\infty/\underset{\sim}{L}$, non-dimensional time

T – temperature

$\underline{u}$ = (u,v), non-dimensional velocity vector

u – non-dimensional velocity component in the x-direction

$\underset{\sim}{u}_\infty$ – inlet velocity

v – non-dimensional velocity component in the y-direction

V – volume

W = $u-iv$, complex velocity

x,y – non-dimensional Cartesian space coordinates

Z = $x+iy$, complex position coordinate in the physical plane

γ = $\int \xi dy$, circulation per unit length

Γ = $\int \xi dA$, circulation

δ – Dirac delta function

δ_s – thickness of the numerical shear layer

Δ – source strength

ε – local rate of expansion

ζ – complex position coordinate in the transformed plane

η – Gaussian random variable

μ – dynamic viscosity

ν – T_b/T_u, temperature, or specific volume ratio

ξ = $\underline{\nabla} x \underline{u}$, vorticity

ρ – density

σ – $\sqrt{2k/R}$, standard deviation

κ – equivalence ratio

ϕ – velocity potential

ψ – stream function

∇^2 – Laplacian operator

Subscripts

b – burned medium

c – cell

f – flame front

i – point in space

j – vortex element

p – potential flow produced by $\underset{\sim}{u}_{\infty}$

s – source velocity

u – unburned medium

ε – produced by combustion

ξ – produced by turbulence

σ – due to combustion

Superscript

~ – complex conjugate

INTRODUCTION

Numerical analysis of turbulent flow has been traditionally based on some form of finite difference treatment of appropriately averaged Navier-Stokes equations, supplemented by an adequate set of relations to correlate the turbulent flow parameters--the closure model. For this purpose it is customary to apply first the Reynolds splitting principle to all the dependent variables. Each term in the governing equations is then appropriately averaged. This may involve either time, or ensemble, or Favre mass averaging, depending on whether one is seeking a steady state, or a time dependent, or a compressible flow solution. Due to the non-linear nature of these equations, double correlations of the fluctuating components arise, while the averaging process involves essentially an integration, as a consequence of which a certain loss of information is incurred. The usual way to remedy this situation is to introduce a system of relations between these correlations and some mean flow parameters--the closure relations. To obtain a numerical solution, a finite difference technique is then applied, yielding the description of the flow field in terms of discrete values of its parameters on the nodes of a Eulerian mesh.

The ACDM (the Averaging-Closure-Differencing Method described above) has been used in a multitude of variations, producing satisfactory results in good agreement with experimental data for a wide assortment of turbulent flow problems. Work in this field has been reviewed recently by Mellor (1979), McDonald (1979), and, with particular reference to modern methods based on the use of PDF (the

Probability Density Function), by Williams and Libby (1980), demonstrating the value of ACDM as a powerful analytic tool for the study of turbulent combustion.

However ACDM is handicapped by a number of drawbacks. Of this, the following are particularly relevant to the problem at hand:

(1) The averaging process deprives the equations of essential information about the mechanism of turbulence; this necessitates the introduction of turbulence models on heuristic grounds rather than obtaining information about them from the solution.

(2) The turbulence model required for the closure relations has to be postulated and the value of its parameters have to be adjusted to match experimental data.

(3) The finite difference technique introduces numerical diffusion which tends to smooth out local perturbations, an effect that is especially harmful at high Reynolds numbers when regions of substantial shear arise in the flow field; the effect of ACDM in this respect is to curtail the Reynolds number, causing the misrepresentation of some of the most essential features of the flow field.

(4) The effects of exothermic processes of combustion on the flow field are particularly difficult to handle by ACDM; as pointed out over 5 years ago by Williams (1974), these processes cause many-fold increases in specific volume and occur at rates which are relatively so high that taking them properly into account in a finite difference scheme is associated with practically insurmountable difficulties.

All these drawbacks are especially catered to by RVM (the Random Vortex Method) developed by Chorin (1973). This method was designed to develop a satisfactory approximation to the solution without differencing the equations. Essential features of the flow field governed by the Navier-Strokes equations are mimicked by the action of vortex elements that model the essential ingredients of turbulence, the elementary eddies. Their random walks express the effects of diffusion, while compliance with the tangential boundary condition at the walls is assured by creation of vorticity in the proper amount. A potential flow solution is used at the same time in accordance with the principle of fractional steps to guarantee that the normal boundary condition is satisfied.

The RVM keeps track of the position and strength of all the vortex elements constituting the flow field and is thus essentially grid-less. It is therefore devoid of the smoothing intrinsic to the finite difference technique and unaffected by the numerical diffusion it introduces. Above all RVM does not involve any averaging whatsoever. On the contrary, instead of damping the disturbances, it actually introduces a certain amount of randomness, or numerical noise, simulating the mechanism of local perturbations in a way similar to the one which occurs in real flow.

Partial convergence proofs for RVM have been provided by Chorin et al. (1978) and Hald (1979). In particular, the error in the solution was shown to be proportional to the inverse of the square root of the Reynolds number, furnishing further evidence of the eminent

suitability of RVM to the analysis of turbulent flows. Its success in this respect has been amply demonstrated by solutions obtained for flows around solid bodies (Chorin, 1973; Cheer, 1979), shear layer effects, Ashurst (1979a, 1979b) and internal flows, McCracken and Peskin (1980). As pointed out by Roshko (1976), it was indeed instrumental in revealing the mechanics of large scale turbulence patterns, the so-called "coherent structure," by elucidating such features as the shear layer mechanisms, processes of eddy shedding, their growth, intertwinning, and pairing.

The most prominent aspects of RVM are presented here from an entirely pragmatic point of view. The algorithm, augmented to accommodate the effects of flames, is then applied to the analysis of turbulent flow with combustion stabilized in the recirculation zone behind a step.

Salient features of such a flow field are displayed in Fig. 1, a selection of cinematographic schlieren records presented by Ganji and Sawyer (1979). The large scale vortex pattern characteristic of the "coherent structure" is clearly discernible, while flame front is recorded by dark streaks, loci of maximum gradient in refractive index reflecting the rapid change in density and temperature due to combustion. The records were obtained for a propane-air mixture at an equivalence ratio of 0.57, initial temperature of 295°K flowing at a velocity of 13.6 m/sec (Reynolds Number 2.2×10^4) in the inlet channel, 2.54 cm wide, into a test section 5.08 cm wide, and 17.3 cm deep. There are two sequential series made out of extracts from the

same high speed movie. The one on the left shows the process of the coalescence of eddies and their intrusion into the recirculation zone at time intervals of 1.22 msec between frames. Displayed in the column on the right side is the normal formation, and development of eddies in the mixing zone at time intervals of 1.16 msec.

The analysis is restricted by a formidable array of simplifying idealizations. However, it should be stressed, this is not tantamount to restrictions of the RVM itself. The principal raison d'etre for our idealizations is simplicity. As for the first practical application of a new method to combustion, it is indeed obvious that the simplest case is most appropriate. It serves as the point of departure for the treatment of more complicated situations and moreover simplicity has a definite bearing on the economy of computation. The techniques we can develop on the basis of the simple case should be of benefit to future work on more involved problems.

PROBLEM

According to the arguments prescribed in the Introduction, the problem we treat is formulated on the basis of the following idealizations:

(1) the flow is two-dimensional i.e., strictly planar;

(2) the flowing substance consists only of two incompressible media, the unburned mixture and the burned gas;

(3) the flame is treated as a constant pressure deflagration acting as an interface between the two media, and propagating locally at a prescribed normal burning velocity;

(4) the exothermicity of combustion is manifested entirely by an increase in specific volume associated with the transformation of one component medium into the other.

Thus completely neglected are, respectively, the following physical phenomena:

(1) three-dimensional effects, in particular vortex stretching;

(2) compressibility effects, in particular acoustic wave interactions;

(3) chemical kinetic effects and molecular diffusion, in particular the flame structure, as well as the influence of the state and composition of reactants on its propagation velocity;

(4) thermal effects, in particular all the thermodynamic properties of the substance and the heat transfer processes.

It should be noted that the above is consistent with the well known model of thin flame, or infinitely fast kinetics, used widely for the analysis of mixed controlled turbulent combustion.

As a consequence of these idealizations, the continuity and the Navier-Stokes equations governing the flow field can be expressed in the following simple form:

$$\underline{\nabla}\cdot\underline{u} = \varepsilon(\underline{r}_f) \tag{1}$$

$$\frac{D\underline{u}}{Dt} = R^{-1}\nabla^2\underline{u} - \underline{\nabla}p \tag{2}$$

where $\underline{u} = (u,v)$ is the velocity vector normalized by the inlet velocity $\underset{\sim}{u}_\infty$, ε is the corresponding local rate of expansion, $\underline{r} = (x,y)$ is the position vector normalized by $\underset{\sim}{L}$, the reference length, t - the time normalized by $\underset{\sim}{L}/\underset{\sim}{u}_\infty$, R - the Reynolds Number and - the pressure normalized by $\rho\underset{\sim}{u}_\infty$, ρ denoting the reference density of the medium, subscript f refers to the flame front, while

$$\frac{D}{Dt} \quad \frac{\partial}{\partial t} + \underline{u}\cdot\underline{\nabla}$$

is the substantial derivative, ∇^2 - the Laplacian and $\underline{\nabla}$ is the usual del or nabla operator.

The flow field is specified by the solution of these equations, subject to the boundary conditions

$$\underline{u} = 0 \qquad \text{along all solid boundaries} \tag{3}$$

$$\underline{u} = (1,0) \qquad \text{at inlet} \tag{4}$$

The distribution of ε is determined by the location of the flame frong, $\underline{r}_f$, which is governed by the flame propagation equation

$$\frac{D\underline{r}_f}{Dt} = S_u \underline{n}_f \tag{5}$$

where S_u is the normal burning velocity, while $\underline{n}_f$ is the unit vector normal to the flame surface.

PROCEDURE

The procedure is based on the principle of fractional steps (viz. e.g., Lie, 1889; Samarski, 1962) according to which the governing equations are split into a sum of elementary components and the solution is determined by treating these components in succession.

The essential element used for this purpose is the vorticity

$$\xi = \underline{\nabla} \times \underline{u} \tag{6}$$

which is introduced by expressing Eq. (2) in terms of its curl, the vortex transport equation,

$$\frac{D\xi}{Dt} = R^{-1}\nabla^2\xi \tag{7}$$

while, it should be recalled, $\underline{\nabla} \times \underline{\nabla}p = 0$.

The flow is thus described by Eqs. (1), (6) and (7).

Equation (1) and (6) are used to determine the velocity field, $\underline{u}(\underline{r})$, while, in accordance with the principal feature of RVM, Eq. (7) is employed to update the vorticity field, $\xi(x,y)$. Then $\varepsilon(x,y)$ is determined by the flame propagation algorithm we developed for the solution of Eq. (5).

Thus $\underline{u}$ is decomposed into a divergence free vector field $\underline{u}_\xi$ and a curl free field $\underline{u}_\varepsilon$ where

$$\underline{u} = \underline{u}_\xi + \underline{u}_\varepsilon \tag{8}$$

In doing this we exploit the Hodge decomposition theorem (viz. Batchelor, 1969; Chorin and Marsden, 1979). The governing equations

for $\underline{u}_\xi$ and $\underline{u}_\varepsilon$ are then obtained immediately by the substitution of Eq. (8) in Eqs. (1) and (6).

$$\underline{\nabla} \cdot \underline{u}_\xi = 0 \tag{9}$$

$$\underline{\nabla} \times \underline{u}_\xi = \xi \tag{10}$$

and

$$\underline{\nabla} \cdot \underline{u}_\varepsilon = \varepsilon \tag{11}$$

$$\underline{\nabla} \times \underline{u}_\varepsilon = 0 \tag{12}$$

Both $\underline{u}_\xi$ and $\underline{u}_\varepsilon$ are required to satisfy to zero normal velocity boundary condition independently, namely

$$\underline{u}_\xi \cdot \underline{n} = 0 \tag{13}$$

$$\underline{u}_\varepsilon \cdot \underline{n} = 0 \tag{14}$$

where $\underline{n}$ is the unit vector normal to the walls.

However, only the total velocity, $\underline{u}$, is required to satisfy the no-slip condition

$$\underline{u} \cdot \underline{s} = 0 \tag{15}$$

where $\underline{s}$ is the unit vector tangent to the walls.

The structure of the algorithm is described schematically in form of a block diagram in Fig. 2. There are two loops, one for handling vortex dynamics, and the other for flame propagation. These are linked together to yield the total velocity field. Key elements in the first loop are vortices, transported by diffusion and convection, the fractional steps of Eq. (7). Key elements in the second loop are volume sources, monitored by advection and combustion, the fractional steps of Eq. (5).

VORTEX DYNAMICS

The mechanism of turbulence is described in essence by vortex dynamics. This process is evaluated here by first determining the velocity field $\underline{u}$, that is produced by a given vorticity distribution, (x,y), according to Eqs. (9) and (10) with the zero normal velocity boundary condition, Eq. (13), and then updating the vorticity field in accordance with the vortex transport equation, Eq. (7), implementing at the same time the no-slip boundary condition, Eq. (15).

As the principal feature of RVM, the flow field is expressed for this purpose in terms of discrete elements, the so-called vortex blobs and vortex sheets. Their properties are presented here in turn.

(a) Vortex Blobs

In order to derive the properties of vortex blobs, Eq. (10) is expressed in terms of the stream function, ,

$$\nabla^2\psi = -\xi \tag{1.1}$$

where

$$u = \frac{\partial\psi}{\partial y} \quad ; \quad v = -\frac{\partial\psi}{\partial x} \tag{1.2}$$

so that Eq. (9) is satisfied exactly.

The velocity is then described in terms of

$$\xi_j = \Gamma_j \, \delta(\underline{r} - \underline{r}_j) \tag{1.3}$$

where δ is the Dirac delta function and

$$\Gamma_j = \lim_{\Delta A_j \to 0} \int_{\Delta A_j} \xi_j \, dA \tag{1.4}$$

is the circulation of a vortex ar $\underline{r}_j$, while ξ_j is acting on area ΔA_j. The solution of Eq. (1.1) is expressed by the Green's function

$$G(\underline{r},\underline{r}_j) = \frac{\Gamma_j}{2\pi} \log|\underline{r} - \underline{r}_j| \tag{1.5}$$

representing the field of a potential vortex.

Equation (1.5) can then be used to construct a solution to Eq. (1.1) for a general distribution of ξ in the form

$$\psi(x,y) = \int_A G(\underline{r},\underline{r}_j) \, \xi(\underline{r}_j) \, dA \tag{1.6}$$

where A is the area of the flow field. The above integral can be evaluated as a sum of all the contributions of ξ, after it had been partitioned into discrete elements ξ_j. The elementary vorticity, ξ_j, is a function of small support that tends to a delta function as the area where it exists, ΔA_j, approaches zero. This process requires smoothing of the function in Eq. (1.5) to eliminate the singularity at its center (Chorin, 1973). Thus, the integral in Eq. (1.6) becomes

$$\psi = \sum_j G_j \Gamma_j \tag{1.7}$$

in which case

$$\Gamma_j = \int_{\Delta A_j} \xi_j \, dA$$

where ΔA_j is finite, while G_j is the corresponding smooth Green's function at $\underline{r}_j$ (Chorin, 1973; Hald, 1980).

The elementary component of the flow field specified by Eq. (1.7) is called a vortex blob. The volicity field it produces in free space, i.e., one without boundaries, is obtained by substituting Eq. (1.5) into Eq. (1.2) and smoothing G around the center. For this purpose it is written, using complex variables, as follows:

$$W_\psi(Z,Z_j) = \frac{-i\Gamma_j|Z - Z_j|}{2\pi \mathrm{Max}(|Z - Z_j|, r_o)} \frac{1}{(Z - Z_j)} \tag{1.8}$$

where $W = u - iv$, $i = \sqrt{-1}$, $Z = x + iy$ while r_o is the cut-off radius, i.e., the radius of the core within which $|\underline{u}|$ is constant, in compliance with the smoothing requirement for the function expressed by Eq. (1.5). The velocity distribution of a blob is displayed in Fig. 3.

In order to satisfy the boundary condition given by Eq. (13) we use conformal mapping to transform the flow field into the upper-half ζ-plane, and add the velocity produced by the image of vortex ζ_j. The corresponding velocity field in the ζ-plane produced by a vortex blob at ζ_j is thus given by

$$W_\xi(\zeta,\zeta_j) = W_\psi(\zeta,\zeta_j) - W_\psi(\zeta,\tilde{\zeta}_j) \tag{1.9}$$

where $W_\psi(\zeta,\zeta_j)$ is given by Eq. (1.8).

The boundary condition of Eq. (4) is taken care of by the velocity $W_p(\zeta)$ of the potential flow produced by a unit velocity at the inlet. The total velocity produced by a set of J_b vortex blobs, including the effect of flow at the inlet, is thus

$$W_\xi(\zeta) = W_p(\zeta) + \sum_{j=1}^{J_b} W_\xi(\zeta,\zeta_j) \tag{1.10}$$

To deduce the solution in the physical domain, the Z-plane, one applies then the Schwarz-Christoffel theorem to specify the differential of the transform function

$$\frac{d\zeta}{dZ} = F(\zeta) \tag{1.11}$$

for a given geometry of the flow field. Since then

$$W(Z) = W(\zeta)\ F(\zeta) \tag{1.12}$$

the velocity vector, $\underline{u}_\xi$, in Eq. (8) is thus determined.

The vorticity, $\xi(x,y)$, is updated at every computational time step, k, by solving Eq. (7) in fractional steps made up of the contribution of the convention operator

$$\frac{D\xi}{Dt} = 0 \tag{1.13}$$

and that of the diffusion operator

$$\frac{\partial \xi}{\partial t} = R^{-1}\nabla^2\xi \tag{1.14}$$

According to Eq. (1.13), vortex blobs move at appropriate particle velocity specified by Eq. (8).

The solution corresponding to a time step, k, of a one-dimensional component of the diffusion equation, Eq. (1.14), when the initial condition is given by the Dirac delta function, $\delta(0)$, is the Green's function

$$G(x,k) = \left(\frac{4\pi k}{R}\right)^{-1/2} \exp\left(-\frac{Rx^2}{4k}\right) \tag{1.15}$$

This is the probability density function of a Gaussian random variable with zero mean and a standard deviation of $\sigma = \sqrt{2k/R}$! Thus, if the initial vorticity is split into a set of discrete vortex elements and each of them is given a displacement from the origin by an amount drawn from a set of Gaussian random numbers of an appropriate variance, it provides an approximation to Eq. (1.15) by sampling. When a general distribution of vorticity $\xi(x)$ is given, the exact solution after time k of Eq. (30) is

$$\gamma(x) = \int_A G(x-x',k)\, \xi(x')\, dx' \tag{1.16}$$

where γ denotes the circulation per unit length, while G is given by Eq. (1.15). The probabilistic counterpart of this solution is obtained by displacing each vortex element from its position x' through a distance n_i. The random walk is then constructed by repeating this procedure at each time step.

Two-dimensional random walk is treated in essentially the same way, the vortex elements being moved in two normal directions x and y, by two independent Gaussian random variables with zero mean and a standard deviation of $\sigma = \sqrt{2k/R}$.

The convection and diffusion contributions in the Z-plane are combined, according to Eq. (7) by the summation

$$Z_j(t + k) = Z_j(t) + \tilde{W}(Z_j)\, k + \eta_j \tag{1.17}$$

where $W = W_\xi + W_\varepsilon$ and $\eta_j = \eta_x + i\eta_y$ or, in the ζ-plane by using its transform

$$\zeta_j(t + k) = \zeta_j(t) + \tilde{W}(\zeta_j)\, \tilde{F}(\zeta_j)\, F(\zeta_j)k + \eta_j F(\zeta_j) \tag{1.18}$$

Since the velocity is calculated in the ζ-plane by implementing Eq. (1.10) the use of Eq. (1.18) is more straightforward and hence more economical then that of Eq. (1.17).

To satisfy the no-slip boundary condition expressed by Eq. (3), the velocity, W, has to be calculated at a number of points along the wall. The points are selected to be a distance h apart along each wall. Wherever the tangential velocity u_W at wall is not zero, a vortex with a circulation $u_W h$ is created and included in the computations at the next time step, according to Eq. (1.17) or Eq. (1.18). However, this procedure of vorticity creation is not accurate since on the average one half of the newly created blobs is lost through diffusion across the wall. This implies that Kelvin's theorem

is not satisfied exactly and the accuracy near the wall is poor. Furthermore, vortex blobs do not provide a good description of the flow near solid walls where velocity gradients are very high, because inside the core of a blob the velocity is considered to be constant. This motivates the introduction of vortex sheets to take up the role of blobs in shear layers at the walls.

(b) Vortex Sheets

If we take x to be the direction along a wall and y the normal to it, the following two conditions are known to prevail in the shear layer immediately adjacent to it:

1. $\partial v/\partial x \ll \partial u/\partial y$ (1.19)
2. diffusion in the x-direction is negligibly small in comparison to convention in this direction.

A vortex element constructed on the basis of these conditions is referred to as the vortex sheet.

As a consequence of Eq. (1.19), Eq. (10) is reduced to

$$\xi = -\frac{\partial u}{\partial y} \tag{1.20}$$

The above, in conjunction with Eq. (9), determines $\underline{u}_{\xi}(\underline{r})$ as follows. Integrating Eq. (1.20) from $y = \delta_s$, the outer edge of the numerical shear layer at the wall, to y_i, one obtains,

$$u_{\delta}(x_i) - u(x_i,y_i) = -\int_{y_i}^{\delta_s} \xi \, dy \tag{1.21}$$

where u_{δ} is u at $y = \delta_s$.

The above integral can be transformed into a summation by partitioning the value of ξ along y and defining the circulation of a vortex sheet per unit length as

$$\gamma_j = \lim_{\Delta y \to 0} \int_{y_i}^{y_i + \Delta y} \xi \, dy \tag{1.22}$$

If a sheet has a length h, then its circulation, Γ_j, is

$$\Gamma_j = h \, \gamma_j \tag{1.23}$$

and from Eqs. (1.21) and (1.22) the velocity jump across it, Δu_j, per unit sheet length is

$$\Delta u_j = \gamma_j \tag{1.24}$$

Unlike the "elliptic" flow modeled by vortex blobs, where the effect of each blob extends throughout the field, as a consequence of Eq. (1.21) the zone of influence of a vortex sheet is restricted to the "shadow" below it, as indicated by the regions marked by right-hand slants in Fig. 4. Thus, the flow velocity at a point (x_i, y_i), where $y_i < y_j$ is determined by the relation

$$u(x_i, y_i) = u_\delta(x_i) - \sum_j \gamma_j d_j \tag{1.25}$$

a summation counterpart of Eq. (1.21) according to Eqs. (1.22) and (1.24) while

$$d_j = 1 - \frac{|x_i - x_j|}{h}$$

is the influence factor of sheet j on point i, expressing the fraction of its length extending over the zone of dependence over point i, indicated by left-hand slants in Fig. 4.

The value of v is determined by the integration of the expression

$$v = -\frac{\partial}{\partial x}\int_0^{y_i} u\, dy \tag{1.26}$$

obtained from Eq. (9) using $u(x_i,y_i)$ as evaluated from Eq. (1.24).

For this purpose one introduces

$$I = \int_0^{y_i} u\, dy = u(x_i)\, y_i - \int_0^{y_i} y\, du = u(x_i)\, y_i - \sum_j \gamma_j d_j y_j \tag{1.27}$$

where, taking advantage of Eq. (1.24), Δu has been replaced by $\gamma_j d_j$. In finite difference form, Eq. (1.26) becomes then

$$v(x_i,y_i) = -\frac{I^+ - I^-}{h} \tag{1.28}$$

where, according to Eq. (1.27), using Eq. (1.25) for $u(X_i)$,

$$I^{\pm} = u_\delta(x_i \pm \frac{h}{2})\, y_i - \sum_j y_j^* \gamma_j d_j^{\pm} \tag{1.29}$$

while, as indicated in Fig. 4,

$$d_j^{\pm} = 1 - \frac{(x_i \pm \frac{h}{2} - x_j)}{h}$$

and

$$y^* = \text{Min}(y_i, y_j)$$

The motion of the sheets is governed by an equation identical to Eq. (1.17), but with $\underline{u}$ evaluated from Eq. (1.25) and Eq. (1.29) while $n_i = 0 + i n_y$, in accordance with condition (2) stated at the beginning of this section. To make sure that the motion of a vortex sheet is matched with the vortex blob it can generate, a correction term has to be added to Eq. (1.25) in order to account for the effect of the image of the blob. According to Chorin (1978), this is equal to $-1/2\ \gamma_j$. A number of techniques to reduce the statistical error and speed up the convergence of the vortex sheet algorithm has been suggested by Chorin (1978).

(c) Algorithm

The above concepts are implemented as follows:

First the value of h, the sheet length specifying the spatial resolution, is chosen. The value of the time step, k, is then fixed in accordance with the Courant stability condition, $k \leq h/\max \underline{u}$ (Chorin, 1980a). For a given Reynolds number, this specifies the standard deviation σ. The thickness of the numerical shear layer δ_s is then taken as a multiple of σ whereby, as shown in Fig. 5, the loss of vortex blobs due to their random walk is minimized. Finally, the number of sheets initially in the stack is chosen, limiting the maximum allowable value for γ.

At time zero only the incoming flow $u_p(\zeta)$ exists. The resulting velocity along the wall is fixed by the potential flow solution of Eq. (1.1). The displacement of the sheets in the numerical shear layer is then calculated, using Eq. (1.17) with velocity specified by Eq. (1.25) and Eq. (1.28). The various possibilities that may occur due to vortex sheet displacement are illustrated in Fig. 5. When a sheet gets out of the boundary layer, it becomes a blob with a total circulation adjusted according to Eq. (1.23).

The core radius, r_o, is then fixed in such a way that the no-slip boundary condition is satisfied. To do so with a minimum error, one sets $r_o > \delta_s$. The velocity at the wall produced by the blob and its image is then, in accordance with Eq. (1.9),

$$u_o = \frac{\Gamma_j}{\pi r_o}$$

whence, by virtue of Eq. (1.23) and (1.24) with $\Delta u_j = u_o$,

$$r_o = \frac{h}{\pi} \tag{1.30}$$

providing an explicit relation between the length of the vortex sheet and the core radius of a vortex blob.

If a sheet gets out on the other side of the wall, it becomes restored by its mirror image either in the shear layer as a sheet or in the flow field as a blob, as depicted in Fig. 5.

Corresponding displacements of vortex blobs are calculated by the use of Eq. (1.18) with their velocities evaluated from Eq. (1.10). Again, Fig. 5 displays the various ways in which a blob can be transformed into a sheet. The last possibility of losing a vortex blob is minimized by the right choice of δ_s, as already pointed out.

Once the position and strength of both the sheets and blobs are established, the flow field at a given time step is fully determined. It should be noted that vortex blobs appear only as a consequence of the displacement of vortex sheets outside the boundary layer, modeling the mechanism of the generation of turbulence under actual flow conditions.

(d) Results

The Z-plane and ζ-plane for flow over a rearward facing step are presented in Fig. 6. The functions W_p and F are

$$W_p(\zeta) = \frac{H}{\pi\zeta} \tag{1.31}$$

and

$$F(\zeta) = \frac{\pi\zeta}{H}\left(\frac{\zeta - 4}{\zeta - 1}\right)^{1/2} \tag{1.32}$$

where, as shown in Fig. 6, H is the height of the channel.

The results of computations for turbulent flow behind a step of the same geometrical proportions as Fig. 1, corresponding to Reynolds Number of 10^4 at inlet, or for 2.54 cm width of the channel in the

experimental apparatus, $\underset{\sim}{u}$ = 6 m/sec, are shown in Fig. 7. Included there are two sequential series of computer outputs. The one on the left describes the development of the flow field by presenting vortex velocity vector fields tracing the motion of all the vortex blobs included in the solution at successive time intervals, each equal to 50 computational steps of 0.1 H/2 $\underset{\sim}{u}_\infty$ sec. The one on the right shows the growth of a large scale eddy traced at time intervals equal to 5 computational steps.

A velocity vector is represented there, as usual, by a line segment providing information on its magnitude and direction. However, instead of being furnished with the conventional arrowhead, it is attached at its origin to a small circle denoting the location of the vortex blob to which it pertains.

FLAME PROPAGATION

According to Idealization 3, the flame front is treated as an interface across which reactants are transformed into products at a rate controlled by the normal burning velocity. The method used for tracing the motion of such an interface was developed by Chorin (1980) and implemented with the help of the algorithm of Noh and Woodward (1976).

The flow field is divided for this purpose by a grid of mesh size, h_c, into square cells. The fraction of volume, V, occupied in a given cell by the burned medium is expressed in terms of a number

$$f \equiv \frac{V_b}{V_c} \tag{2.1}$$

It is easy to show that

$$f = \frac{\rho_c - \rho_u}{\rho_b - \rho_u} \tag{2.2}$$

where ρ is the density, while subscripts c, u, and b, refer, respectively, to the property of the medium in the cell, the unburned medium, and the burned medium.

Since, by reason of Idealization 3, the flame is treated as a constant pressure deflagration, f can be expressed in terms of the usual reaction progress parameter

$$c = \frac{T_c - T_u}{T_b - T_u} = \frac{1}{\nu - 1}\left(\frac{T_c}{T_u} - 1\right) \tag{2.3}$$

where

$$\nu \equiv \frac{T_b}{T_u} = \frac{\rho_u}{\rho_b} \tag{2.4}$$

while T can be considered to represent either absolute temperature (if the change in molecular weight is negligible) or temperature divided by the molecular weight.

Thus, with the use of the perfect gas equation of state, Eqs. (2.2), (2.3) and (2.4) yield

$$f = \frac{\nu\, c}{1 + (\nu - 1)\, c} \tag{2.5a}$$

whence

$$c = \frac{f}{\nu + (\nu - 1)\, f} \tag{2.5b}$$

specifying, in effect, the temperature distribution, for, as a consequence of Idealization 2, ν = const. throughout the flow field.

Thus, f = 0 or 1 means that there is, respectively, either unburned or burned medium in the cell, while fractional values of f indicate cells containing the interface. Its particular geometry is

deduced, depending on the f numbers in neighboring cells. In this connection, as illustrated in Fig. 8, proper provisions are included in the algorithm for four possibilities:

(a) vertical interface

(b) horizontal interface

(c) rectangular corner

(d) neck

As a consequence, the interface is made up of horizontal and vertical line segments, yielding higher spatial resolution than h_c, the mesh size of the grid.

The motion of the interface, or flame propagation, is described by Eq. (5). By virtue of the principle of fractional steps, its effects are split into two components:

(a) advection, prescribed by

$$\frac{D\underline{r}_f}{Dt} = 0 \tag{2.6}$$

(b) combustion, prescribed by

$$\frac{\partial \underline{r}_f}{\partial t} = S_u \underline{n}_f \tag{2.7}$$

providing proper set-up for the inclusion of the effects of

(c) exothermicity

Algorithms for each of these processes are presented here in sequence.

(a) Advection

The advection step is the passive displacement due to the velocity field. It is evaluated by calculating first the velocity components at mid-points on the sides of the cell, as shown in Fig. 9. The interface is then transported in two fractional steps, one horizontal and one vertical, changing the f-number of the cell by an amount proportional to corresponding displacements in time step, k_c. The algorithm is stable whenever the Courant condition, $k_c \leq h_c/\max|\underline{u}|$, is satisfied (viz. Noh and Woodward, 1976).

(b) Combustion

The combustion step is the advancement of the front due to consumption of the unburned medium. The front moves in the direction of its normal with a relative velocity taken here as a constant, equal to the appropriate laminar burning velocity of the mixture, S_u. The corresponding motion of the interface is evaluated by the implementation of the Huygens' principle using the advection algorithm. At the nth computational step one calculates for this purpose the displacements due to S_u in eight directions: The four sides and four corners of each cell, so that all of its neighbors are affected. For a given cell at (i,j) this results in eight new f-numbers. The value assigned to it is then:

$$f_{ij}^{n+1} = \underset{0\leq \ell \leq 8}{\text{Max}}\, f_{ij}^{(\ell)} \qquad (2.9)$$

where $\ell = 1, \ldots 8$, while $f_{ij}^{(0)} = f_{ij}^{n}$. It should be noted that the algorithm provides in effect information on the displacement of the interface due to its motion at a given velocity normal to its frontal surface, without having to determine its actual direction (viz. Chorin, 1980).

(c) Exothermicity

Mechanical effects of the exothermic process are manifested by volumetric expansion behind the flame front. The velocity field induced thereby is governed by Eqs. (11) and (12) and Eq. (14).

As in the case of vortex blobs, Eq. (11) and (12) are solved by superposition. A velocity potential, ϕ, is introduced for this purpose, so that

$$u = \frac{\partial \phi}{\partial x} \quad ; \quad v = \frac{\partial \phi}{\partial y} \tag{2.10}$$

satisfying exactly Eq. (12). The governing equation for ϕ,

$$\nabla^2 \phi = \varepsilon \tag{2.11}$$

is obtained then immediately by the substitution of Eq. (2.9) into Eq. (11).

The solution of this equation is given by

$$\phi(\underline{r}) = \int_A G(\underline{r},\underline{r}')\ \varepsilon(\underline{r}')\ dA \tag{2.12}$$

where

$$G(\underline{r},\underline{r}') = \frac{1}{2\pi} \log|\underline{r} - \underline{r}'|$$

is the Green's function.

Following the procedure used for integrating Eq. (1.6), the solution of Eq. (2.12) is approximated by the summation

$$\phi = \sum_j G(\underline{r},\underline{r}_j)\ \Delta_j \tag{2.13}$$

where

$$\Delta_j = \int_{A_j} \epsilon_j\ dA \tag{2.14}$$

while Δ_j is the source strength, the rate of volumetric expansion it induces, while ϵ_j is the Dirac delta function. As before, in order for the summation to converge, the Green's function is smoothed around $\underline{r}_j$.

The concept of a source blob is that conceived in analogy to a vortex blob. The velocity field produced by a source blob is, in effect, the same as that in Fig. 3. Thus, the velocity produced in a free space by a source blob at Z_j is

$$W_\phi(Z,Z_j) = \frac{\Delta_j|Z - Z_j|}{2\pi\ \mathrm{Max}(|Z - Z_j|\ ,\ r_o)} \frac{1}{(\overline{Z - Z_j})} \tag{2.15}$$

The boundary condition expressed by Eq. (14), are satisfied by adding the velocity produced by the image of each source on the other

side of the wall. Thus the total velocity produced by a source blob in the ζ-plane is given by

$$W_\epsilon(\zeta,\zeta_j) = W_\phi(\zeta,\zeta_j) + W_\phi(\zeta,\tilde{\zeta}_j) \tag{2.16}$$

For J_s source blobs, the solution of Eq. (2.12) is then approximated by the summation of the integral in Eq. (2.13) and the corresponding flow velocity is

$$W_\epsilon(\zeta) = \sum_{j=1}^{J_s} W_\epsilon(\zeta,\zeta_j) \tag{2.17}$$

The strength of the source is adjusted so as to provide for the volumetric expansion specified by Δ_j (viz. Eq. (2.14)) preserving mass. In one-dimensional flow, as depicted in Fig. 10,

$$u_s = \frac{S_b - S_u}{2} \tag{2.18}$$

where S_b is the flame speed as seen from the burned side and S_u is the flame speed seen from the burned side, whence, as a consequence of the continuity requirement,

$$S_b = \nu\, S_u \tag{2.19}$$

where

$$\nu \equiv \rho_u/\rho_b$$

one has

$$u_s = \frac{S_u}{2}(\nu - 1) \tag{2.20}$$

The source strength is then

$$\Delta_j = u_s h_c = \frac{S_u h_c}{2}(\nu - 1) \tag{2.21}$$

while the volumetric rate of combustion is given by

$$\frac{dV_\sigma}{dt} = h_c S_u = h_c^2 \frac{df_\sigma}{dt} \tag{2.22}$$

where df_σ/dt is the rate of change in f due solely to combustion. This yields:

$$\Delta_j = \frac{1}{2} h_c^2 (\nu - 1) \frac{df_\sigma}{dt} \tag{2.23}$$

At the same time, with reference to Fig. 3, the source velocity is identified with the velocity of the core

$$u_o = \frac{\Delta_j}{2\pi r_o} \tag{2.24}$$

so that, as a consequence of Eq. (2.20), one obtains

$$\Delta = 2\pi r_0 u_s = \pi r_o S_u(\nu - 1) \tag{2.25}$$

Thus, by virtue of Eq. (2.23), it follows that

$$r_o = \frac{h_c^2}{2\pi S_u k_c}\Delta f_\sigma \tag{2.26}$$

where the time derivative of f has been expressed in terms of the change in f evaluated for a given time step, k_c, by the implementation of the Huygen's principle.

By virtue of Eq. (8), volumetric sources affect the velocity field. In particular, they modify the value of $\underset{\sim}{u}$. This in turn induces changes in the sheet velocities, as evident from Eqs. (1.25) and (1.28), giving rise to new vortex blobs, etc. The whole algorithm is thus interrelated, as described schematically in Fig. 3.

(d) Results

With the use of RVM a solution was obtained for turbulent flow with combustion in the tunnel behind a step, modeling the process recorded photographically in Fig. 1. The exothermicity of the propane-air mixture, with equivalence ratio $\kappa = 0.5$ used then, was for this purpose expressed in terms of the temperature (or specific volume) ratio $\nu = 4.25$, the laminar burning velocity was taken as $\underset{\sim}{S}_u = 12$ cm/sec, while, as before, the velocity at inlet was $\underset{\sim}{u}_\infty = 6$ m/sec corresponding to $R = 10^4$.

An example of the results is presented in Fig. 11. As Fig. 7, it consists of two sequential series of computer outputs, depicting the

variation of vortex velocity vector fields and flame fronts. The flame contour has been delineated for this purpose as a line of demarcation between cells where $f = 0$ and those where $f > 0$. The sequence in the left column depicts the process of ignition in the turbulent flow field of Fig. 7 in a cell located at point (1,1) i.e., on the center line of the tunnel at a disance from the step equal to the width of the inlet channel. The sequence in the right column displays the "steady flow condition" attained at time $\underset{\sim}{t} = 26.102$ $(H/2\underset{\sim}{u}_{\infty})$ sec. following ignition at the left bottom corner, point (0,0), initiated at the moment when the medium was set in motion (hence smaller number of vortex blobs). The number of computational time steps 0.05 $H/2\underset{\sim}{u}_{\infty}$ sec., between the solutions displayed here was 40 for the left column and 4 for the right.

Considering the stringent idealizations on which the computations are based, the agreement between the numerical model and the experimental observations is indeed remarkable. The RVM is evidently capable of reproducing the essential features of the flow field associated with turbulent combustion as observed by schlieren photography, providing thereby a clarification of the essential mechanism of the process. At this stage one cannot expect, of course, more than a qualitative agreement. A quantitative modeling of stochastic turbulent flow parameters has to be left for future study.

CONCLUSIONS

Demonstrated here was the eminent suitability of RVM for the study of the fluid mechanic properties of turbulent combustion. The main advantage of the method is that it is unencumbered by numerical diffusion. Thus, all the instabilities in the flow field, that arise as a characteristic feature of turbulence, can be sustained without any artificial damping, permitting their effects to be traced without undue distortion. Moreover, by using as the building block the mechanical properties of the essential ingredient of turbulence, the elementary eddy, RVM is capable of modeling the intrinsic physical properties of the flow system, subject only to restrictions introduced at the outset by the simplifying idealizations.

As a consequence, the analysis we presented displayed the following features of turbulent combustion:

1. fluid mechanical processes of the formation of large scale turbulent flow structure,

2. rationale for the role played by the intrinsic instability of the flow system in stabilizing the flame--the basic mechanism of a blunt body flame holder,

3. fluid mechanical processes of ignition in turbulent flow of premixed gases,

4. detailed features of entrainment and mixing as principle means for the control of the combustion process,

5. the mechanism of exothermic processes in turbulent combustion.

ACKNOWLEDGMENT

The authors wish to express their appreciation to the Program Director of the Research Project, under which these studies were conducted in part, Dr. C. J. Marek of NASA Research Center for his managerial supervision, encouragement, and support.

APPENDIX I

VORTEX MOTION IN THE TRANSFORMED PLANE

Trajectories of the vortices in the transformed ζ-plane are required in order to evaluate the velocity W(Z) using Eq. (1.10) and Eq. (1.12). This can be obtained by a stepwise conformal mapping of trajectories in the Z-plane, defined by Eq. (1.17), using the inverse of the transformation function $Z = Z(\zeta)$, the integral form of Eq. (1.11)

$$Z(\zeta) = \int \frac{d\zeta}{F(\zeta)} \tag{I.1}$$

which, for the geometry of Fig. 6 is

$$Z = \frac{H}{\pi} \left\{ \log \frac{1 + q}{1 - q} - \frac{1}{2} \log \frac{2 + q}{1 - q} \right\} \tag{I.1a}$$

where

$$q = \sqrt{\frac{4 - \zeta}{1 - \zeta}}$$

However, the inverse of the above

$$\zeta = \zeta(Z) \tag{I.2}$$

is awkward and lengthy to evaluate. Hence one has to resort to numerical methods to integrate Eq. (1.11) directly in order to calculate corresponding displacements in the ζ-plane of those in the Z-plane.

This procedure can be reduced substantially if one uses Eq. (1.18) to trace these vortices in the ζ-plane directly, thus eliminating the use of the Z-plane except for the presentation of the results. This equation is obtained from Eq. (1.12) to write $W(Z)$ in terms of ζ as

$$\tilde{W}(Z) = \widetilde{W(\zeta)\ F(\zeta)} = \tilde{W}(\zeta)\ \tilde{F}(\zeta) \tag{I.3}$$

If $\zeta(t)$ is defined to be the map of $Z(t)$, then

$$\zeta(t) = \zeta(Z(t)) \tag{I.4}$$

and one can write

$$\zeta(t + k) - \zeta(t) = \zeta(Z(t + k)) - \zeta(Z(t))$$

or, taking the first term of the Taylor series expansion,

$$\zeta(t + k) - \zeta(t) = \left\{Z(t + k) - Z(t)\right\} \frac{d\zeta}{dZ} \tag{I.5}$$

If Z is a vortex center, then Eq. (1.17) specifies the change in Z_j. Using Eq. (I.3), Eq. (1.11) and rearranging one obtains Eq. (1.18) as

$$\zeta_j(t + k) = \zeta_j(t) + \{\tilde{W}(\zeta_j)\ F(\tilde{\zeta}_j)\ k + \eta_j\} F(\zeta_j) \tag{I.6}$$

Eq. (I.6), along with Eq. (1.10) provide all the necessary information about the flow field. It is of interest to note that the effect of the geometry of the Z-plane on the motion in the ζ-plane is preserved in terms of F and $\tilde{F}$ in Eq. (I.6).

APPENDIX II

DERIVATION OF EQUATION (2.23)

The total volume created by a set of sources distributed on the surface of a flame should provide for the extra volume on the side of products due to the expansion of reactants as they burn. If the fluid leaves a source with a velocity u_s normal to the surface of the flame, then

$$\frac{dV}{dt} = \int_f u_s \underline{n}_f \cdot d\underline{A}_f \tag{II.1}$$

where dV/dt = rate of volume increase due to the sources and A_f = area of the flame surface. For two dimensional flow, $dA_f = \underline{n}_f dL_f$ where L_f is the length of the flame front and both V and A_f are measured per unit length normal to the plane of the flow. Since u_s is constant for homogeneous systems as indicated by Eq. (2.18), it follows that

$$\frac{dV}{dt} = u_s \int_f \underline{n}_f \cdot \underline{n}_f dL_f = u_s L_f \tag{II.2}$$

The propagation of the flame due to combustion, the reason of volume expansion, is expressed by the left hand side of Eq. (5),

$$\frac{\partial \underline{r}_f}{\partial t} = \underline{n}_f S_u \tag{II.3}$$

When integrating the above equation of the flame surface A_f, it specifies the rate of volume combustion as

$$\int_f \frac{\partial \underline{r}_f}{\partial t} \, d\underline{A} = \int_f S_u \underline{n}_f \, d\underline{A} \tag{II.4}$$

The left hand side of this equation can be written as

$$\frac{dV_b}{dt} = \int_f \frac{\partial \underline{r}_f}{\partial t} \, dA_f = \sum_{i,j} h_c^2 \frac{df_\sigma}{dt} \tag{II.5}$$

i and j cover the whole flow area and the flow is assumed two dimensional. The integral in the right hand side of Eq. (II.4) is evaluated by assuming a constant S_u, yielding a similar expression as that of Eq. (II.2). Thus Eq. (II.4) becomes

$$\sum_{i,j} h_c^2 \frac{df_\sigma}{dt} = S_u L_f \tag{II.6}$$

One can write

$$\frac{dV}{dt} = \sum_{i,j} \Delta_{ij}$$

and by eliminating L_f between Eq. (II.6) and Eq. (2) it follows that

$$\Delta = \frac{u_s}{S_u} h_c^2 \frac{df_\sigma}{dt} \tag{II.7}$$

However, from Eq. (2.18) and Eq. (2.19), one has

$$u_s = \frac{S_u}{2} (\nu - 1)$$

and Eq. (2.23) follows immediately. By using Eq. (II.7), one avoids calculating the flame length as required by Eq. (II.2). Instead one uses the computations of the combustion step in the flame propagation algorithm, described before, to obtain the rate of conversion of reactant's volume due to combustion as indicated in Eq. (II.5).

APPENDIX III

CONSERVATION OF CIRCULATION IN A VARIABLE DENSITY FIELD

The flame front, according to the model presented here, is a constant pressure discontinuity across which a sudden change in density occurs. In the following finite vortices, or vortex blobs, are found to conserve their circulation upon crossing this discontinuity. The proof is limited to two-dimensional situations.

In a two dimensional potential flow, with variable density, the vortex transport equation, (Eq. (2.6) in Chorin and Marsden 1979).

$$\frac{D}{Dt}\,(\xi/\rho) = 0 \tag{III.1}$$

expresses the variation of vorticity with density along a particle path. However, the variation of the circulation, given by

$$\frac{D\Gamma}{Dt} = \frac{D}{Dt}\int \xi\, dA = \frac{D}{Dt}\int (\xi/\rho)\ \rho\, dA \tag{III.2}$$

can be calculated by reversing the integration and differentiation in the above expression as

$$\frac{D\Gamma}{Dt} = \int \frac{D}{Dt}\,(\xi/\rho)\ \rho\, dA + \int \xi/\rho\ \frac{D}{Dt}\,(\rho dA) \tag{III.3}$$

However, ρdA = constant along a particle path and, taking Eq. (III.1) into account,

$$\frac{D\Gamma}{Dt} = 0 \qquad \text{(III.4)}$$

Thus, since vortex blobs follow particle paths, their circulation in a variable density field is invariant.

REFERENCES

Ashurst, W. T. (1979a) Numerical Simulation of Turbulent Mixing Layers via Vortex Dynamics. Proc. of the 1st Sym. on Turbulent Shear Flows, ed. by Durst, et al., Springer-Verlag, Berlin, pp. 402-413.

Ashurst, W. T. (1979b) Vortex Simulation of a Model Turbulent Combustor. Proc. of the 7th Colloquium on Gasdynamics of Explosions and Reactive Systems, in press.

Batchelor, G. K. (1967) An Introduction to Fluid Mechanics. Cambridge University Press, London, xviii + 615 pp.

Chorin, A. J. (1980a) Vortex Models and Boundary Layer Instability. SIAM J. Scientific Stat. Comp. 1, 1-24.

Chorin, A. J. (1980b) Flame Advection and Propagation Algorithms. J. Comp. Phys., in press.

Chorin, A. J. (1973) Vortex Sheet Approximation of Boundary Layers, J. Comp. Phys. 27, 428-442.

Chorin, A. J. (1973) Numerical Studies of Slightly Viscous Flow, J. Fluid Mech., 57, 785-796 .

Chorin, A. J., Hughes, T. J. R., MaCracken, M. F., and Marsden, J. E. (1978) Product Formulas and Numerical Algorithms, Comm. on Pure and Appl. Math., 31, 205-256.

Chorin, A. J. and Marsden, J. E. (1979) A Mathematical Introduction to Fluid Mechanics. Springer-Verlag, Berlin, vii + 205 pp.

Cheer, A. Y. (1979) A Study of Incompressible 2-D Vortex Flow Past a Circular Cylinder. Lawrence Berkeley Laboratory, LBL-9950.

Ganji, A. R., and Sawyer, R. F. (1980) An Experimental Study of the Flow Field of a Two-Dimensional Premixed Turbulent Flame. AIAA Journal (in press).

Hald, O. H. (1979) Convergence of Vortex Methods for Euler's Equations II. SIAM J. Numer. Anal., 16, 5, 726-755.

Lie, S. and Engel, F. (1880) Theorie der Transformationsgruppen 3 Vols., Teubner, Leipzig.

MaCracken, M. and Peskin, C. (1980) Vortex Methods for Blood Flow. J. Comp. Phys., (in press).

McDonald, H. (1979) Combustion Modeling in Two and Three Dimensions--Some Numerical Considerations. Prog. Energy Combust. Sci., 5, 97-122.

Mellor, A. M. (1979) Turbulent-Combustion Interaction Models for Practical High Intensity Combustors. 17th Symposium (International) on Combustion, The Combustion Institute, Pittsburgh, PA, 377-387.

Noh, W. T. and Woodward, P. (1976) SLIC (Simple Line Interface Calculation). Proc. 5th Intern. Conf. Num. Math. Fluid Mechanics, Springer-Verlag, Berlin, 330-339.

Roshko, A. (1976) Structure of Turbulent Shear Flows: A New Look. AIAA Journal 14, 10, 1349-1357.

Samarski, A. A. (1962) An Efficient Method for Multi-Dimensional Problems in an Arbitrary Domain, Zrycisl. Mat. i Mat. Fiz. 2, 787.

Williams, F. A. (1974) A Review of Some Theoretical Considerations of Turbulent Flame Structure. Specialists Meeting on "Analytical and Numerical Methods for Investigation of Flow Field, with Chemical Reaction, Especially Related to Combustion," AGARD PEP 43rd Meetings II, 1, Liege, Belgium, 1-125.

Williams, F. A. and Libby, P. A. (1980) Some Implications of Recent Theoretical Studies in Turbulent Combustion. Turbulent Reacting Flows (Editors), Springer-Verlag, Berlin, Heidelberg, New York AIAA preprint (in press).

FIGURE CAPTIONS

Fig. 1. Cinematographic schlieren records of turbulent combustion stabilized behind a step in a propane-air mixture at an equivalence ratio $\kappa = 0.57$, entering the channel at $\underset{\sim}{u}_\infty$ = 13.6 m/sec (Re = 22 x 10^4) while $T_\infty = 295^\circ K$ (from Sawyer and Ganji, 1980).

(a) growth of a large eddy under the influence of recirculation (time interval between frames: 1.22 msec).

(b) "steady state" propagation of a large scale ("coherent") structure (time interval between frames: 1.16 msec).

Fig. 2. Structure of the algorithm.

Fig. 3. Velocity distribution of a blob.

Fig. 4. Geometry of interdependence in the numerical shear layer

A - zone of dependence over point i

B - zone of influence under sheet j

C - zone of dependence around point i + 1/2

D - zone of dependence around point i - 1/2

Fig. 5. Transformations of vortex elements in and around a numerical shear layer at the wall.

Fig. 6. Streamlines pattern of initial flow in transformed plane and physical plane of a channel with a step expansion.

Fig. 7. Sequential series of computer plots displaying vortex velocity fields in turbulent flow behind a step at inlet $R = 10^4$.

(a) development of the flow field

(b) growth of a large scale eddy

Fig. 8. Elementary components of an interface recognized by the algorithm.

Fig. 9. Velocity components used in the advection algorithm to determine the motion of the interface in cell (i,j).

Fig. 10. Kinematics of the flame front

———————— tangent to the flame front at point i

- - - - - - - - tangents to particle paths at point i

Fig. 11. Sequential series of computer plots displaying vortex velocity fields and flame fronts in turbulent combustion behind a step at $R = 10^4$ while $S_u = 0.02$ and $\nu = 4.25$, corresponding to a propane-air mixture at $\kappa = 0.5$.

(a) ignition at point (1,1) in a fully developed turbulent flow

(b) "steady state" turbulent flame propagation.

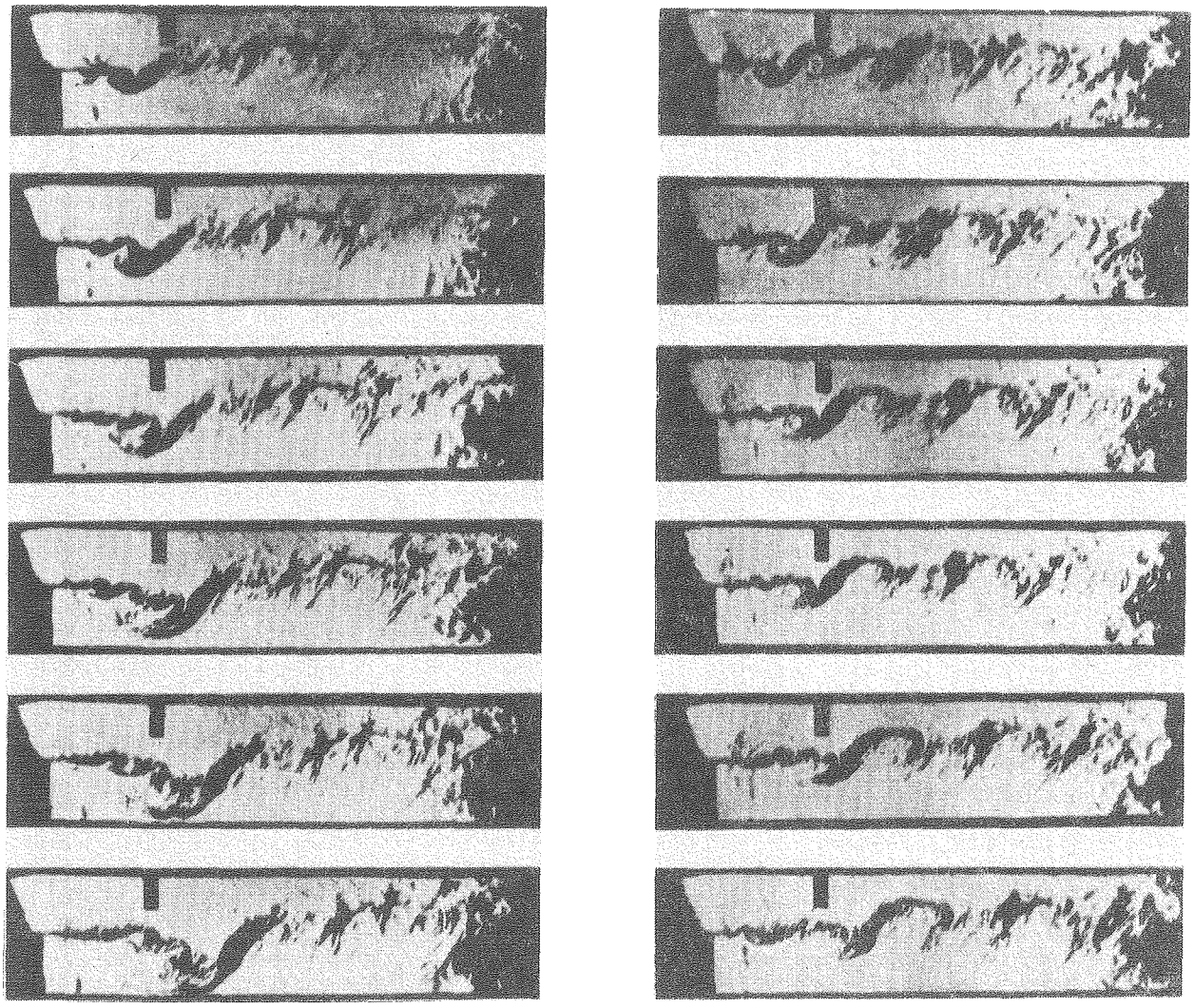

a b

XBB 802 2189

Fig. 1

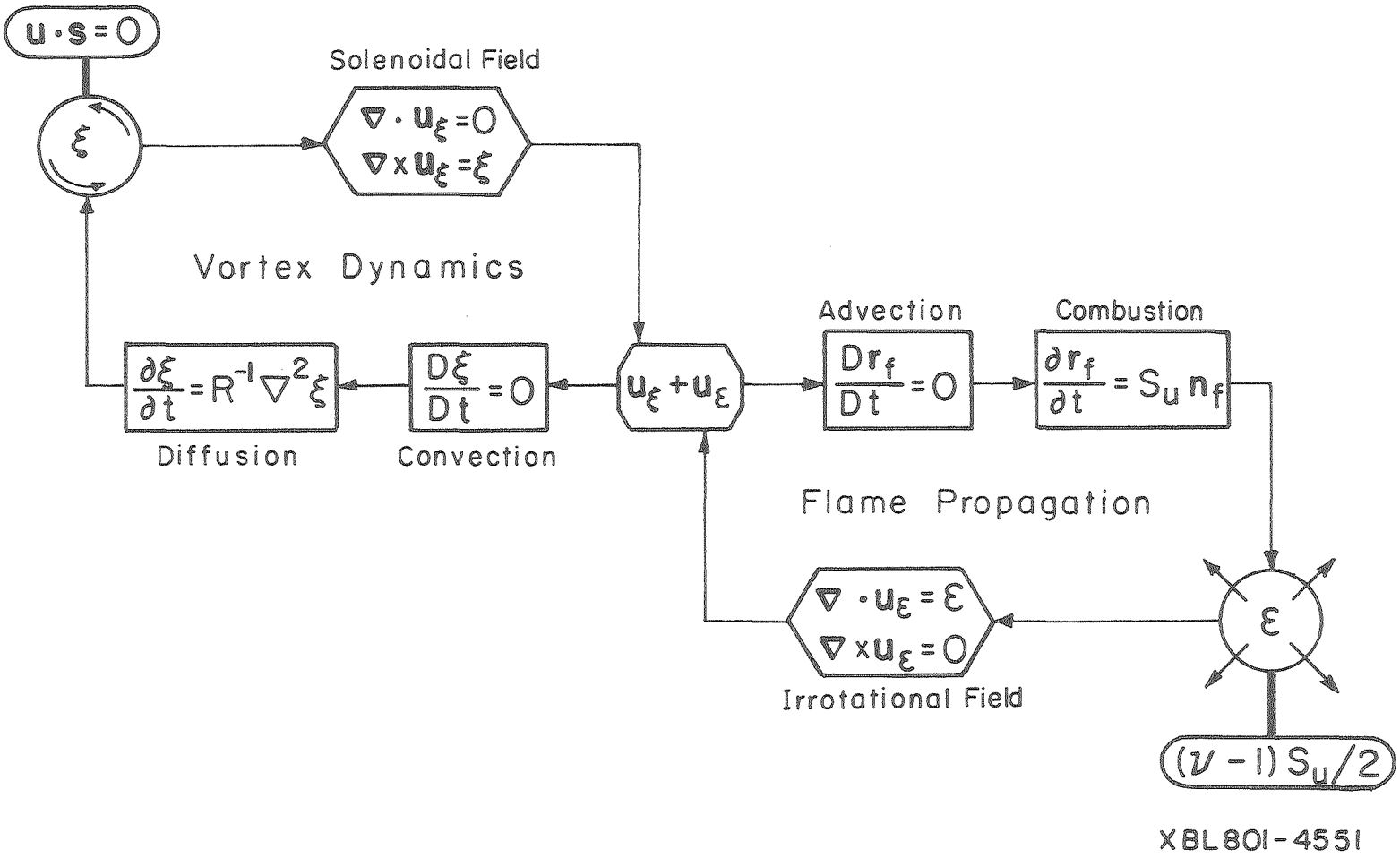
$u \cdot s = 0$
Solenoidal Field
ξ
$\nabla \cdot u_\xi = 0$
$\nabla \times u_\xi = \xi$
Vortex Dynamics
Advection
Combustion
$\frac{\partial \xi}{\partial t} = R^{-1} \nabla^2 \xi$
$\frac{D\xi}{Dt} = 0$
$u_\xi + u_\varepsilon$
$\frac{Dr_f}{Dt} = 0$
$\frac{\partial r_f}{\partial t} = S_u n_f$
Diffusion
Convection
Flame Propagation
$\nabla \cdot u_\varepsilon = \varepsilon$
$\nabla \times u_\varepsilon = 0$
ε
Irrotational Field
$(\nu - 1) S_u / 2$
XBL801-4551

Fig. 2

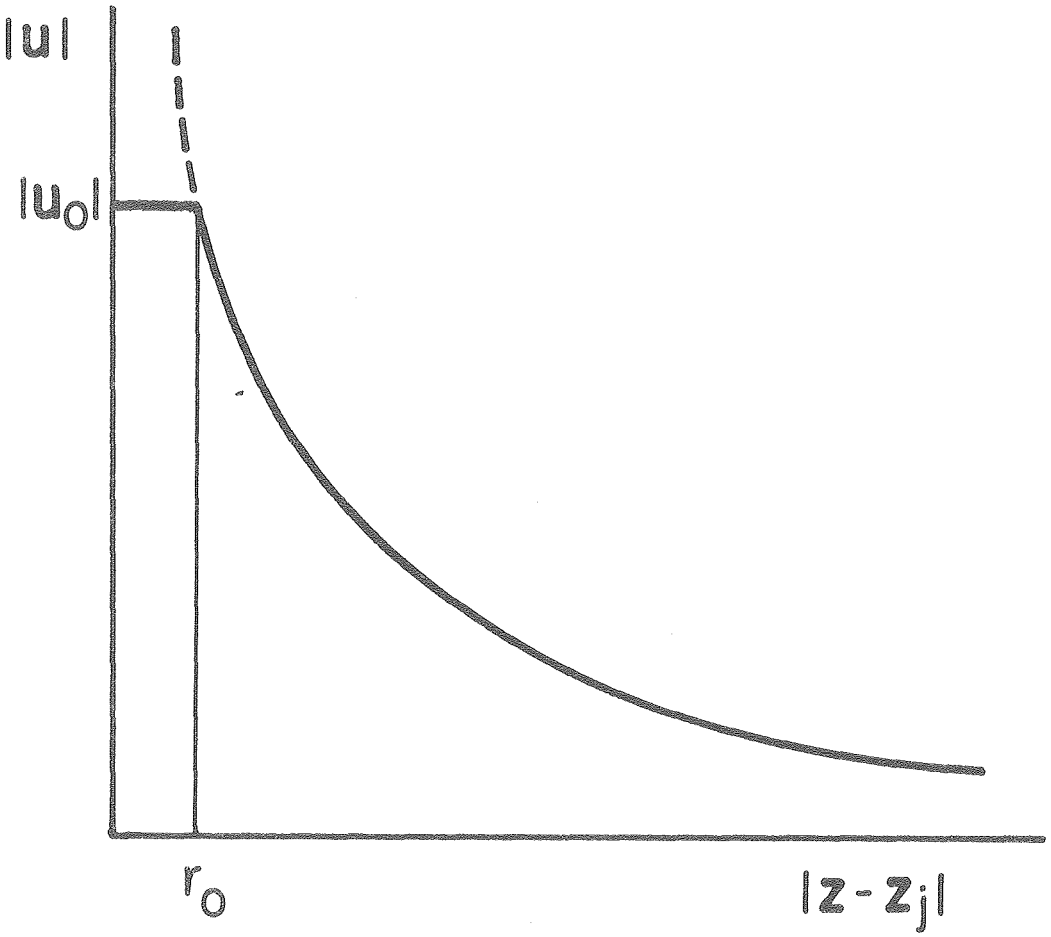

XBL 801-4552

Fig. 3

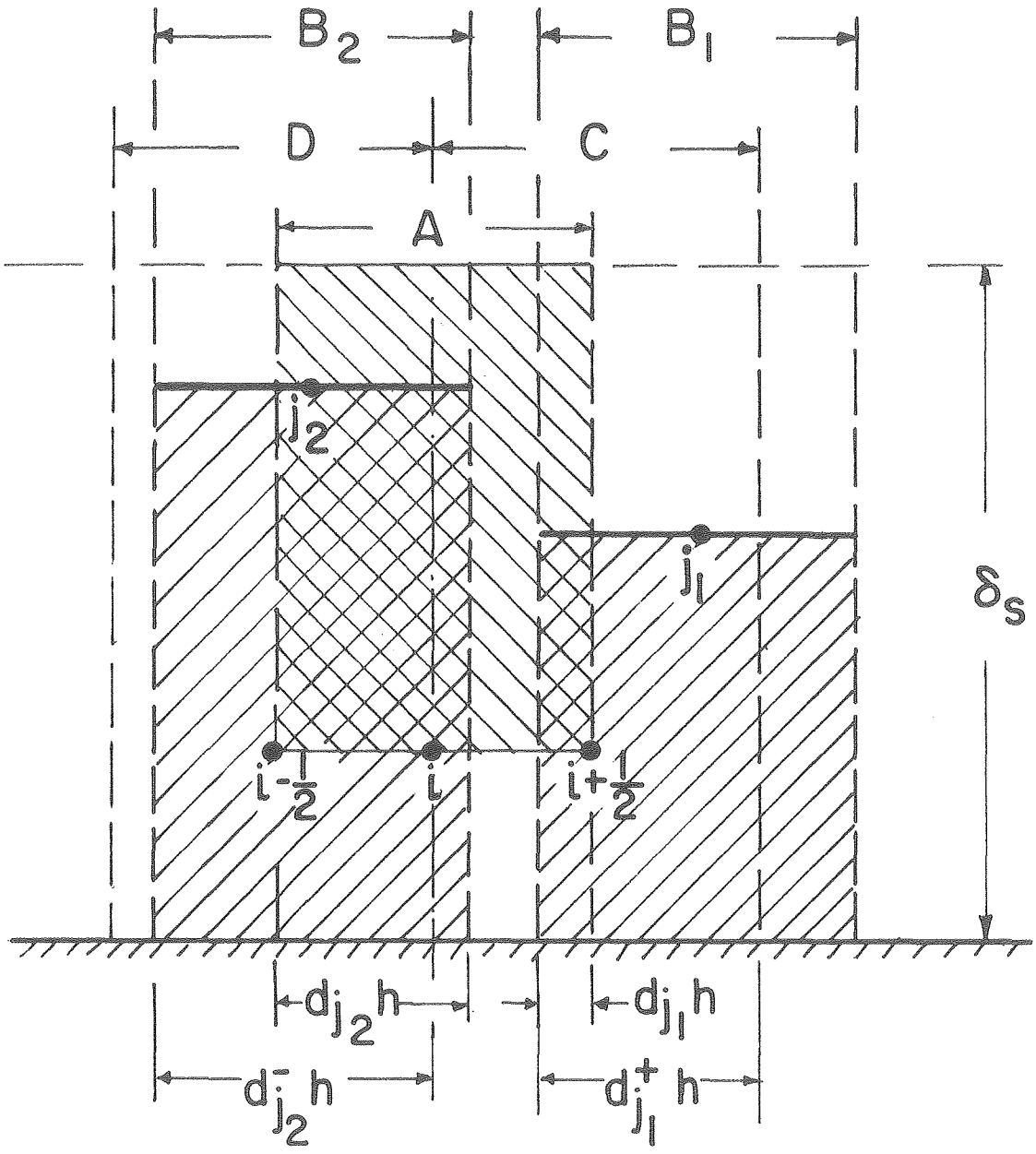

Fig. 4

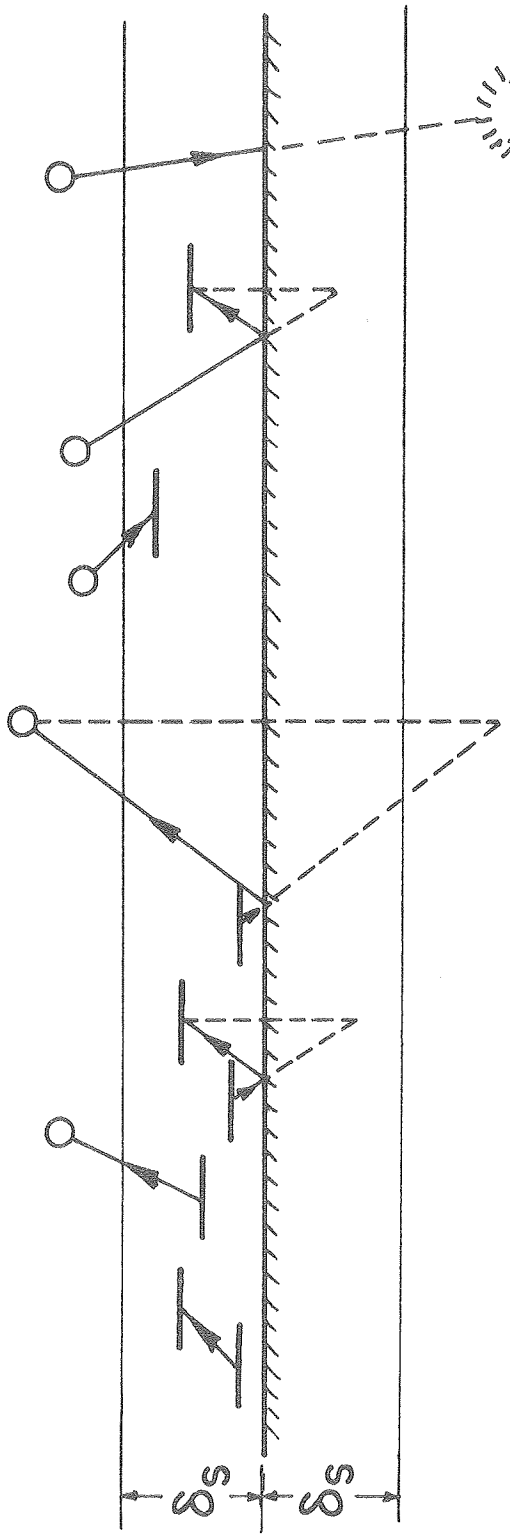

XBL 801-4555

Fig. 5

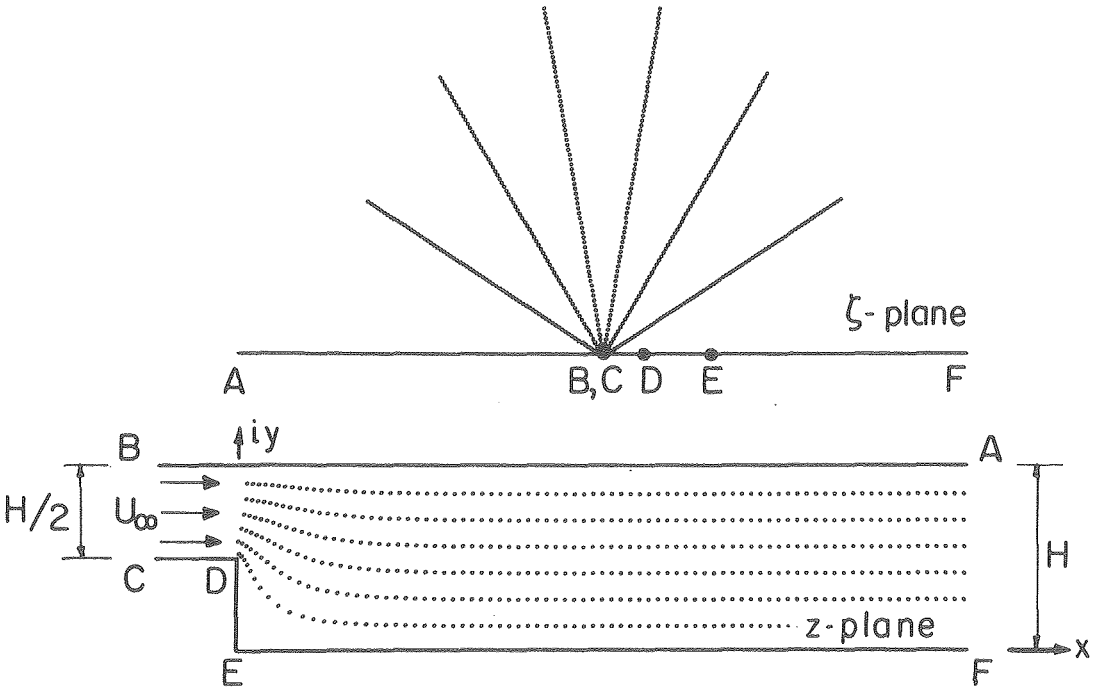

XBL801-4553

Fig. 6

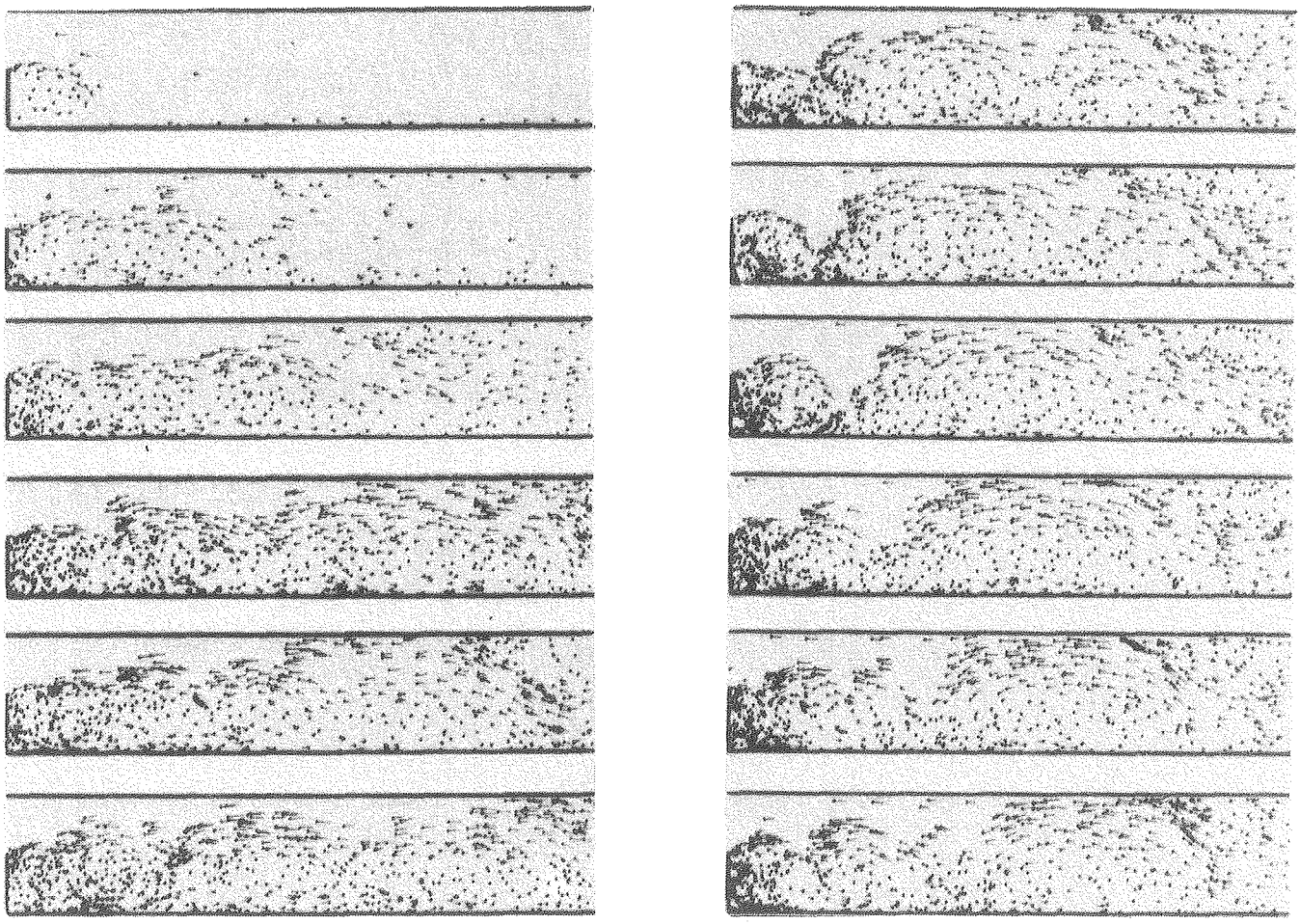

a

b

XBB 802 2188

Fig. 7

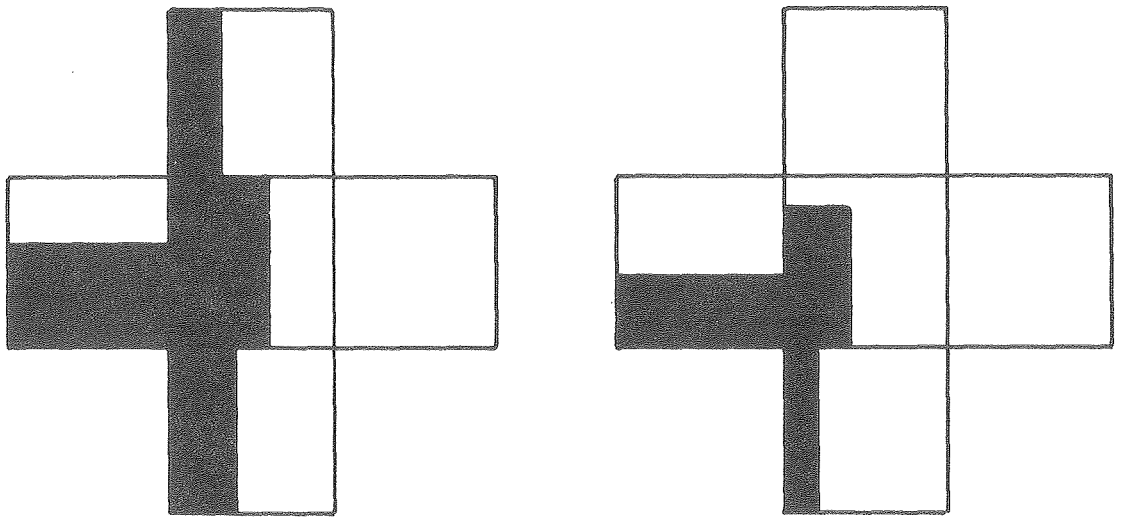

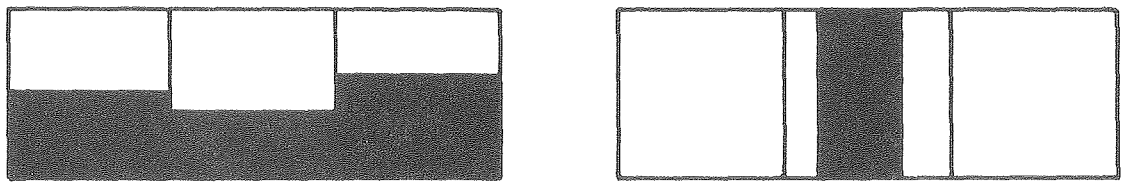

XBL 801-4556

Fig. 8

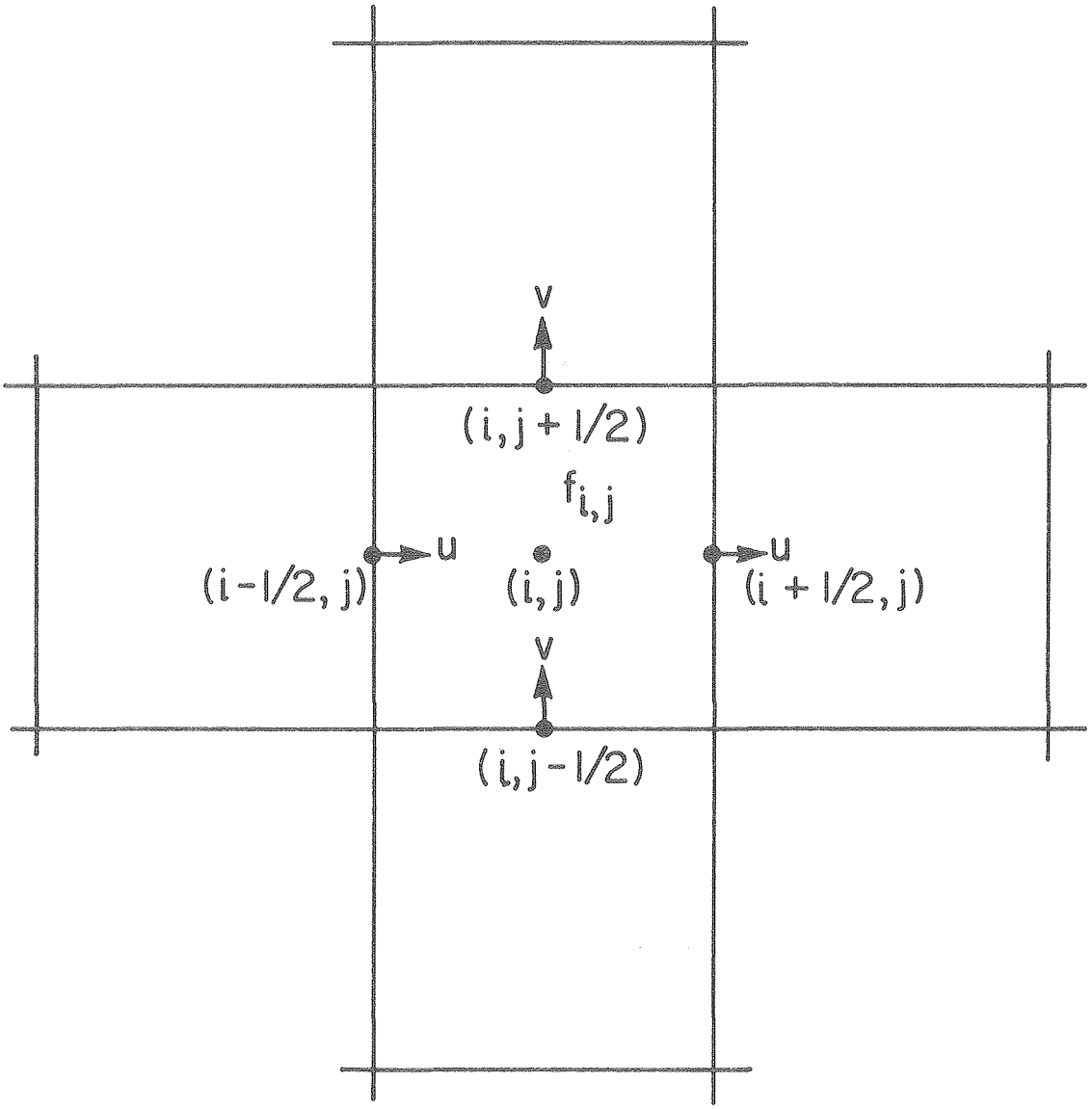

XBL801-4557

Fig. 9

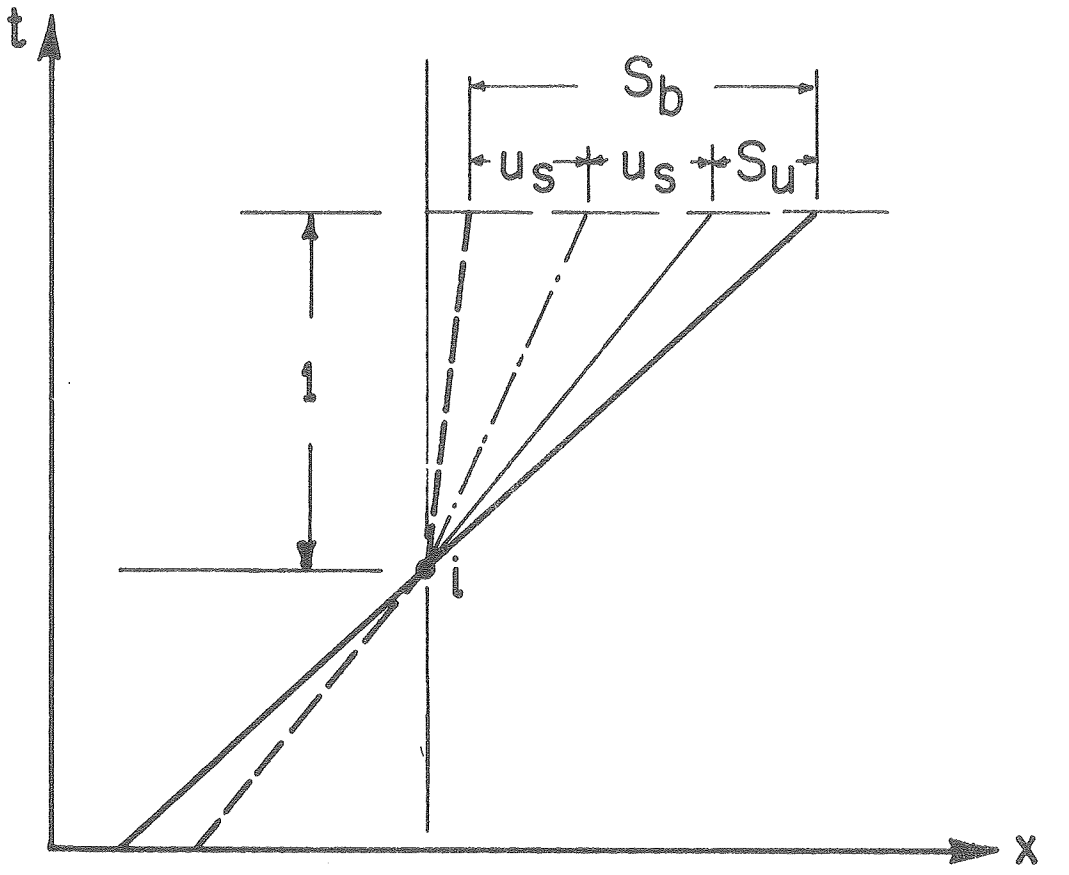

XBL801-4558

Fig. 10

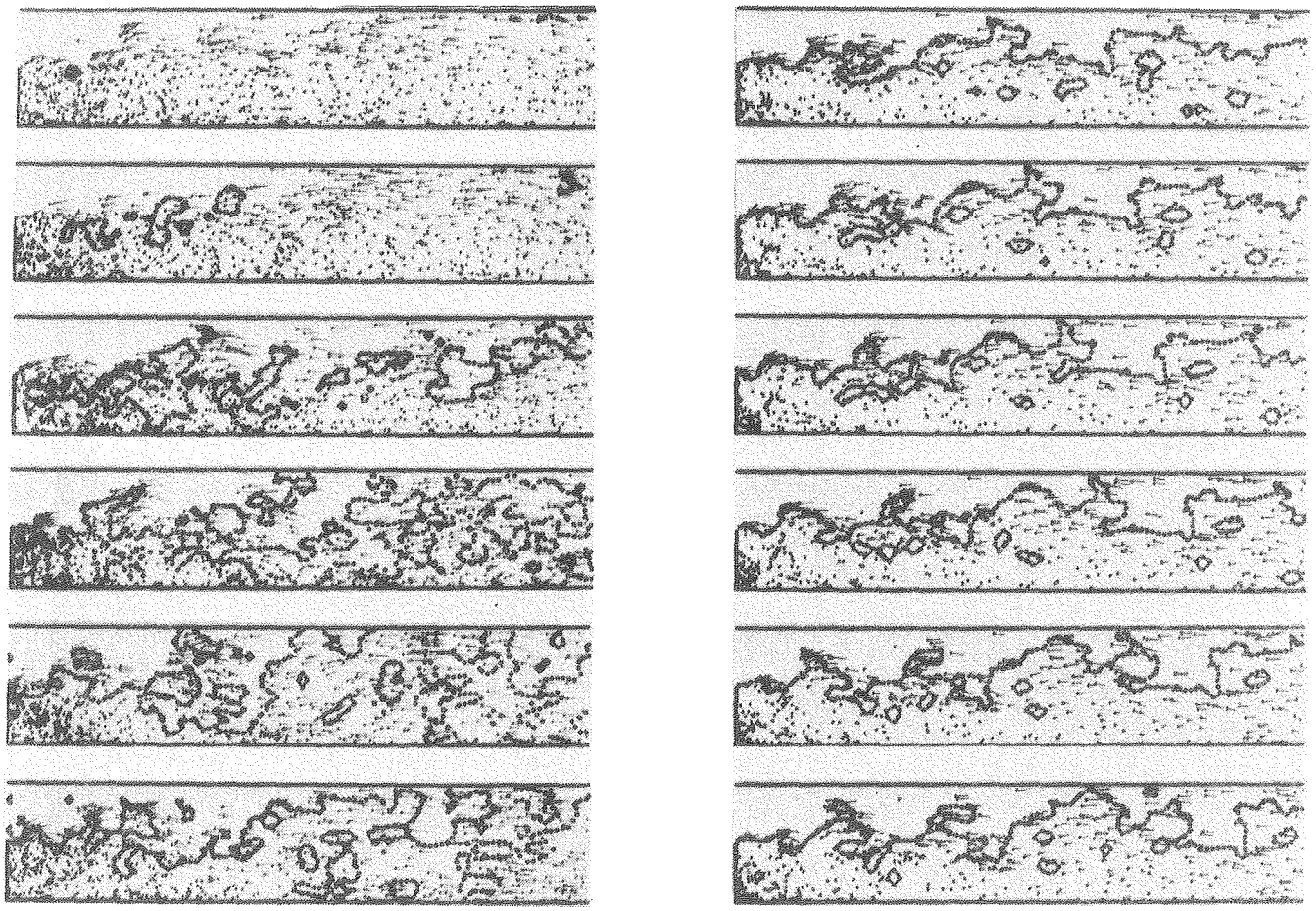

a b

XBB 802 2190

Fig. 11